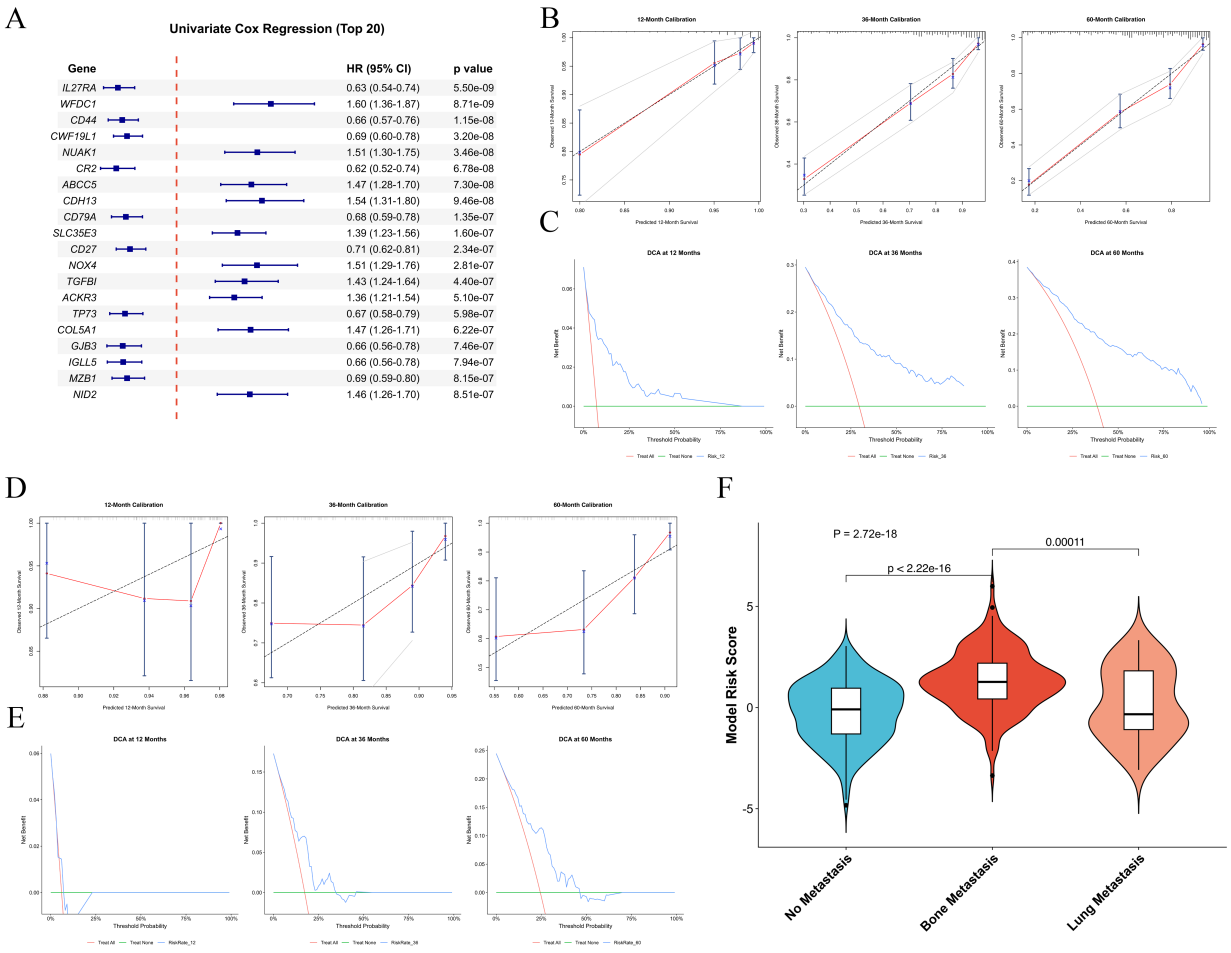

Supplementary Figure 1. Evaluation of the bulk bone metastasis risk model. A) Univariate Cox regression forest plot of the top 20 prognostic genes. B, C) Calibration and decision curve analyses in the training cohort. D, E) Calibration and decision curve analyses in the external validation cohort GSE45255. F) Model risk score across non-metastatic, bone metastatic and lung metastatic samples. Statistical comparisons in F were performed using the Kruskal-Wallis test followed by pairwise comparisons.

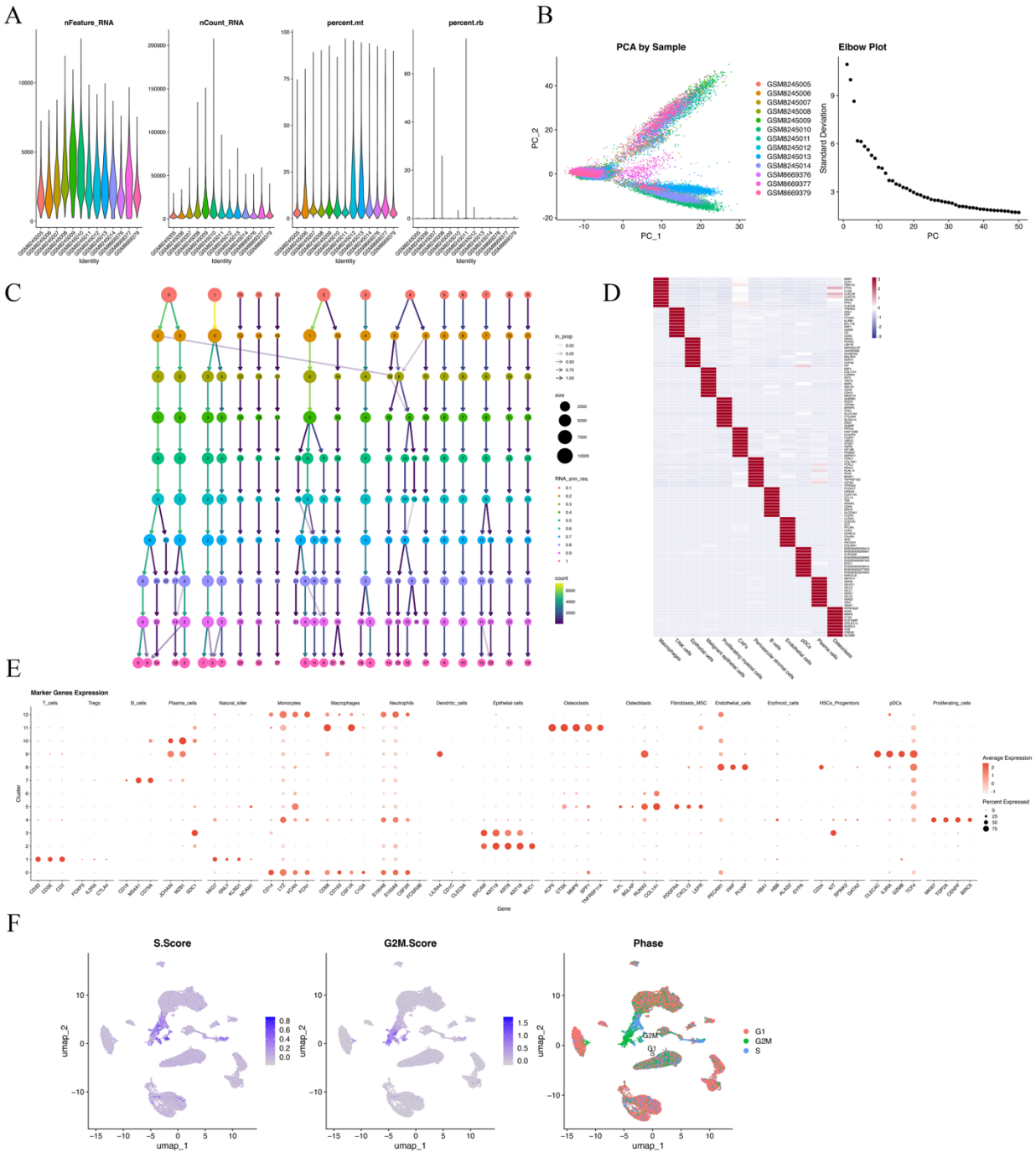

Supplementary Figure 2. Quality control, clustering and annotation support for the single-cell atlas. A) Pre quality control violin plots showing nFeature_RNA, nCount_RNA, mitochondrial transcript percentage and ribosomal transcript percentage across samples. B) Principal component analysis by sample and elbow plot used to guide dimensional reduction. C) Clustree analysis across clustering resolutions. D, E) Marker heatmap and marker gene bubble plot supporting cell type annotation. F) Cell cycle score and phase distribution across the atlas.

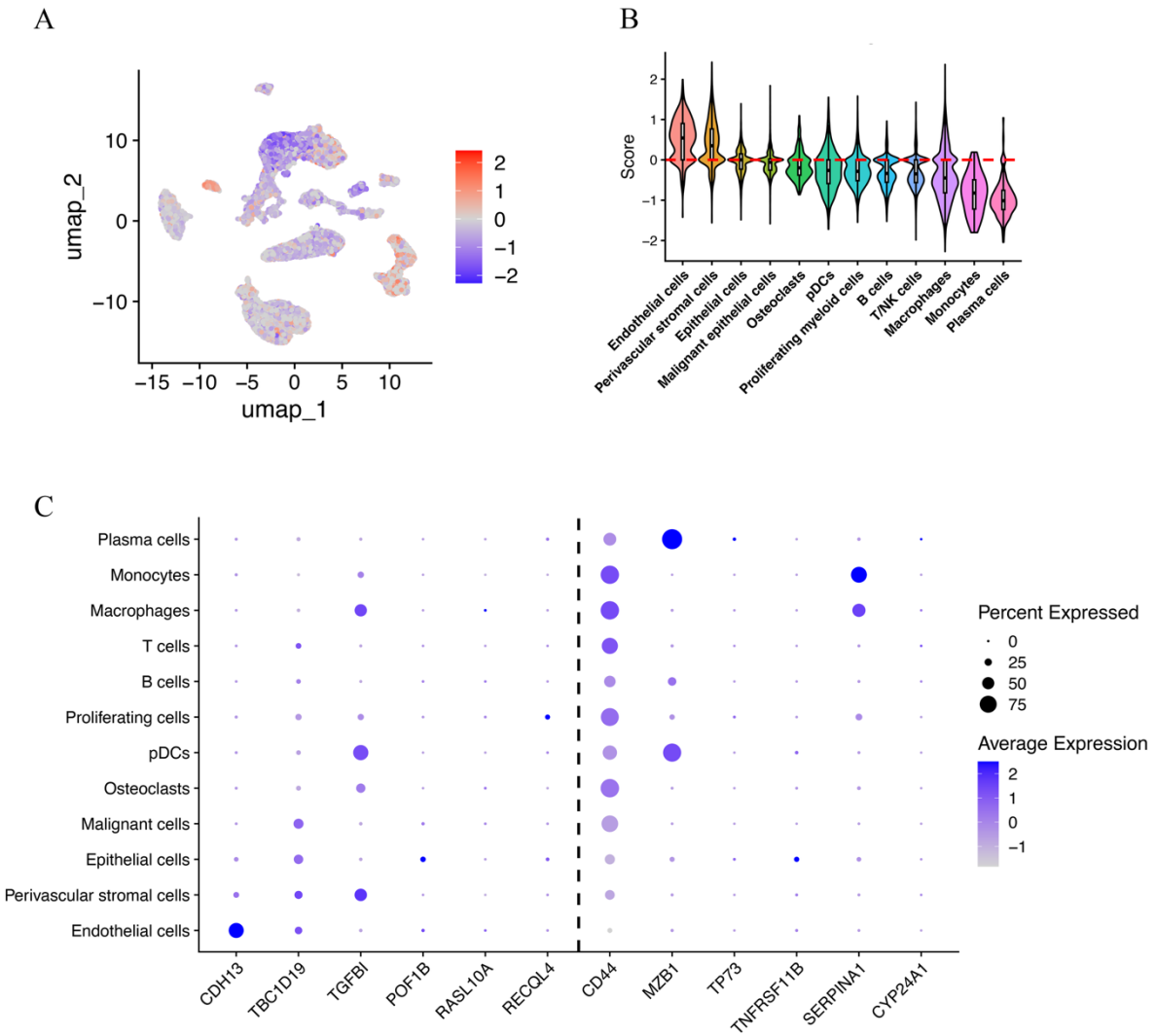

Supplementary Figure 3. Single-cell risk program mapping. A) UMAP visualization of the Cox weighted risk program score. B) Violin plot of the Cox weighted risk program score across annotated cell types. C) Dot plot showing expression of selected model genes across annotated cell types.

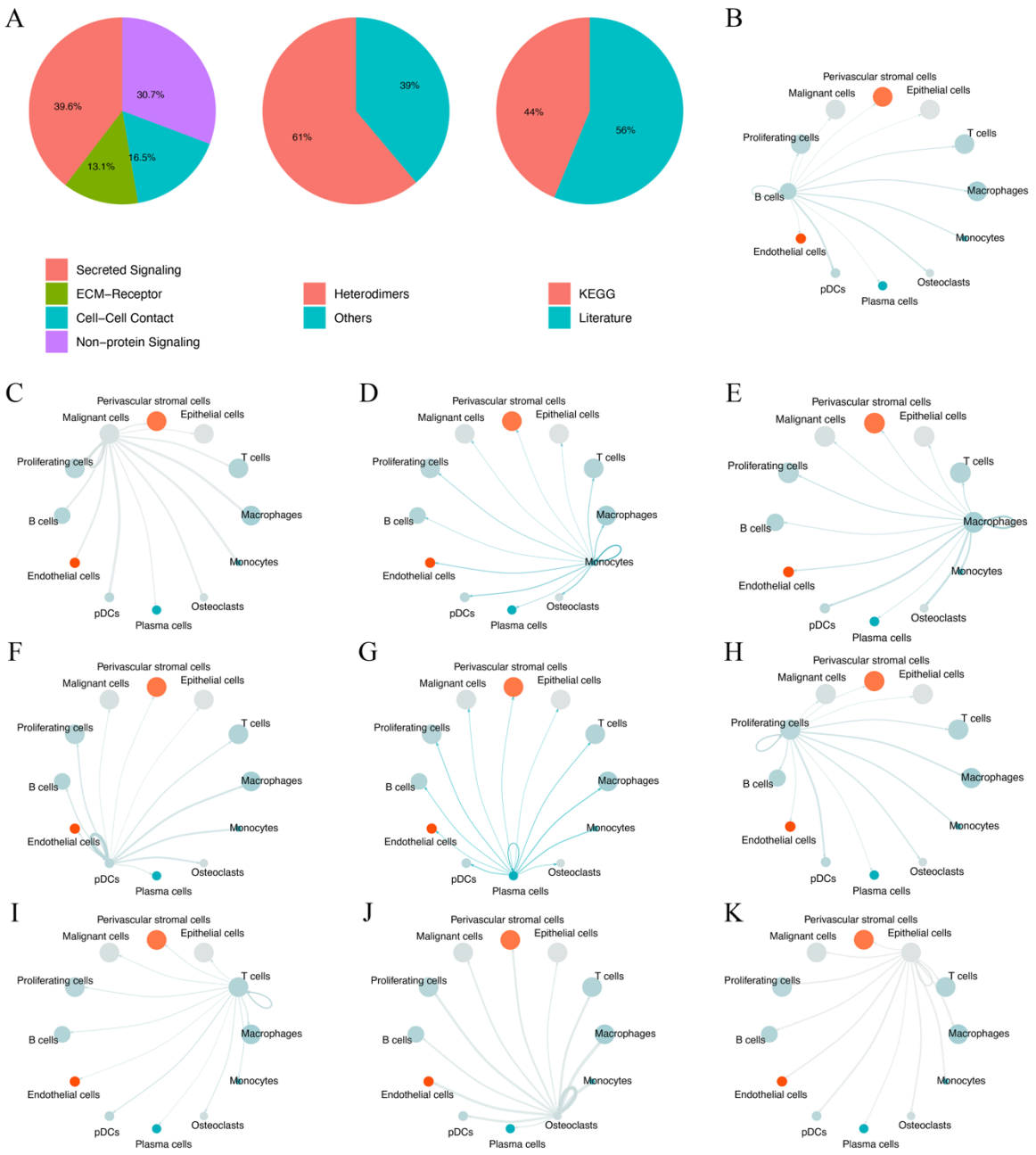

Supplementary Figure 4. CellChat database composition and sender centred communication networks. A) Composition of the CellChat ligand-receptor database represented in the analysis, summarized by interaction category, heteromeric status and evidence source. B-K) Sender centred CellChat network visualizations for major annotated cell types. Node colours indicate the mean Cox weighted risk score, and edge widths indicate inferred communication strength.

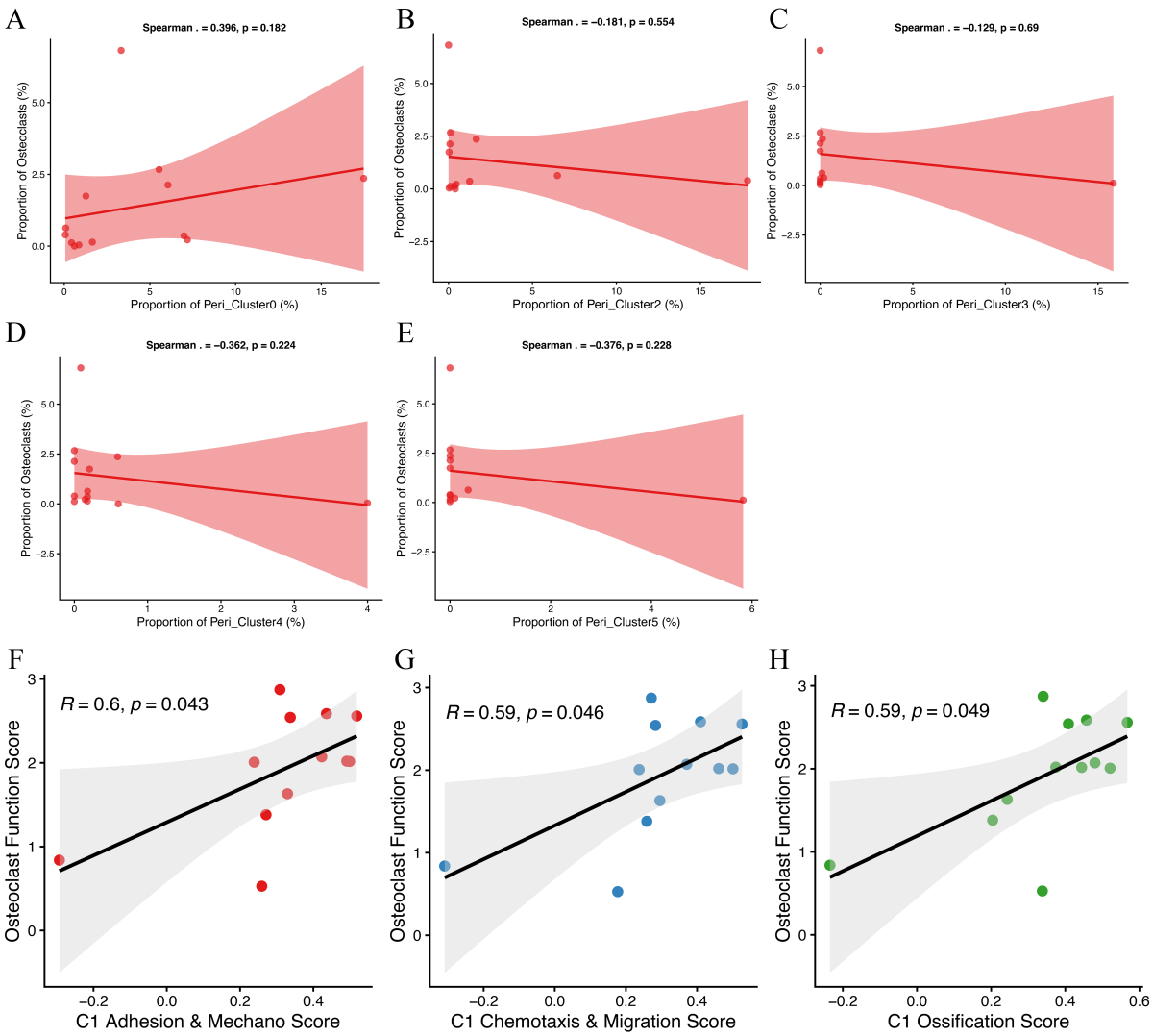

Supplementary Figure 5. Specificity of C1 osteoclast co-occurrence and C1 subprogram associations. A-E) Sample level correlations between osteoclast abundance and individual non-C1 perivascular stromal subcluster abundances. F-H) Correlations between osteoclast function score and C1 adhesion and mechano signalling, chemotaxis and migration, and ossification related subprogram scores. Correlations were assessed using Spearman correlation.

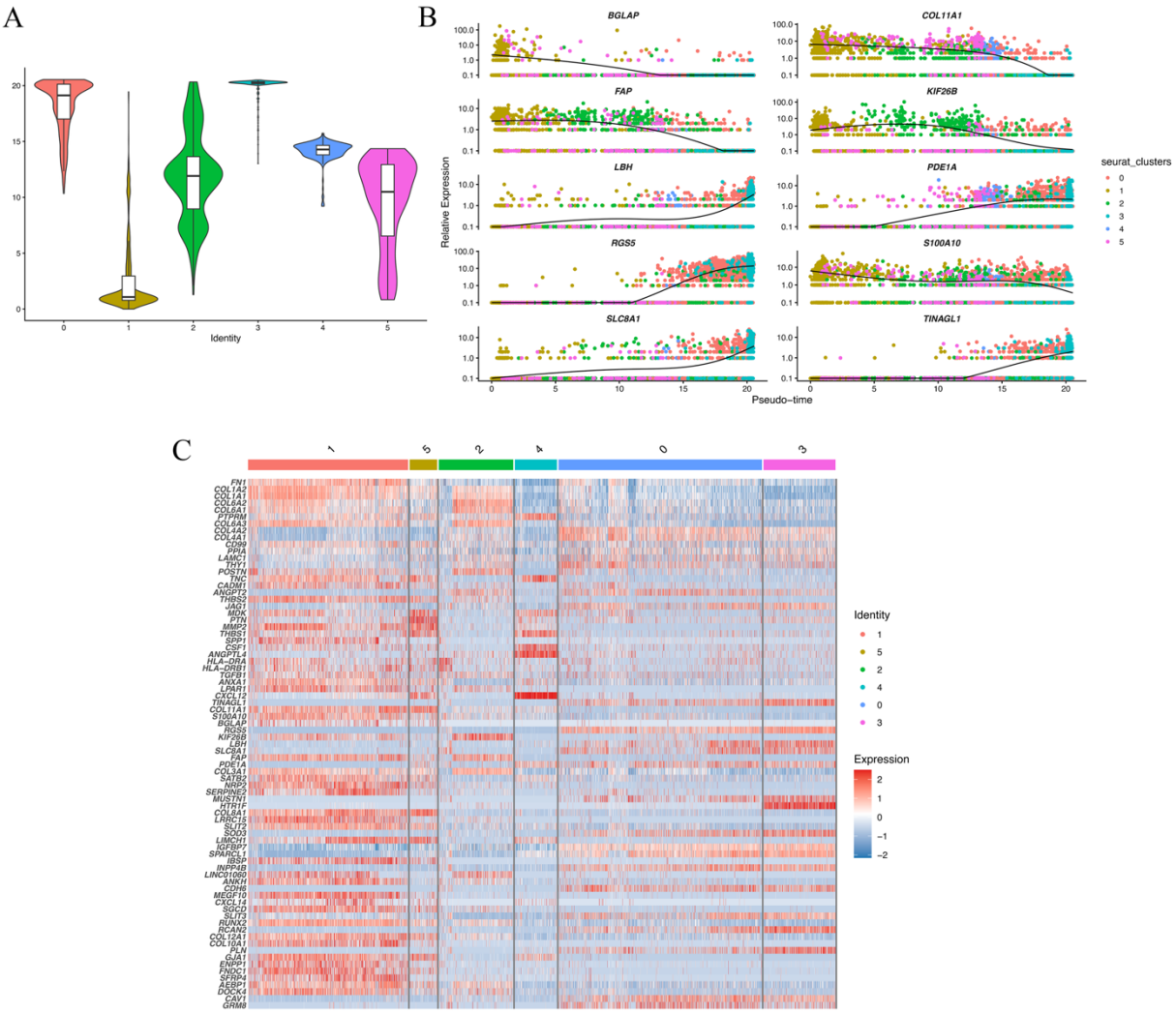

Supplementary Figure 6. Perivascular stromal pseudotime analyses. A) Dynamic expression of top pseudotime associated genes along the perivascular stromal trajectory. B) Pseudotime distribution across perivascular stromal subclusters. C) Heatmap of broader pseudotime associated gene expression programs across perivascular stromal cells.

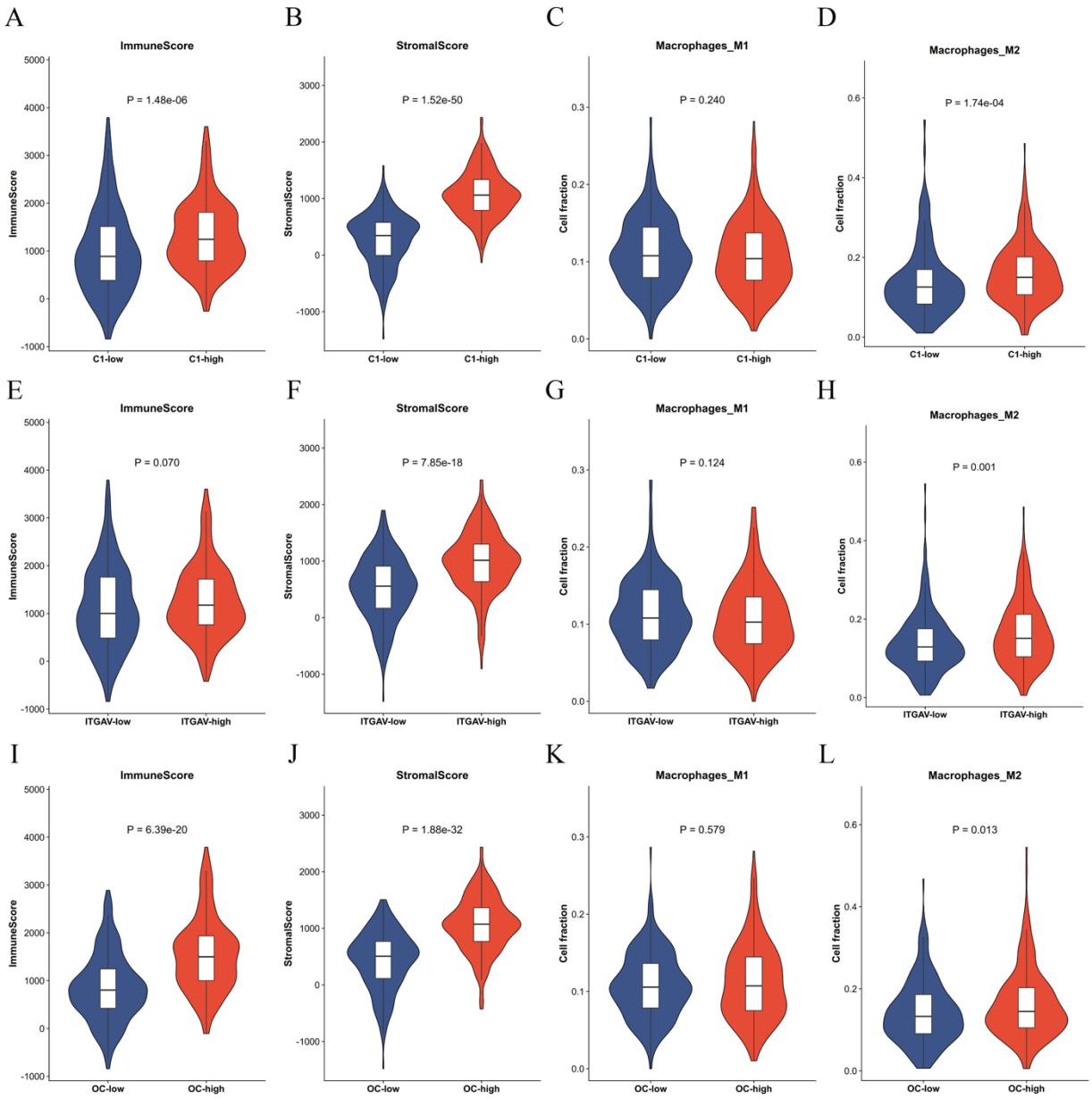

Supplementary Figure 7. Immune and stromal features associated with C1, ITGAV and osteoclast functional states. A-D) ImmuneScore, StromalScore, M1 macrophage fraction and M2 macrophage fraction according to C1 ligand signature status. E-H) The same features according to ITGAV expression status. I-L) The same features according to osteoclast function signature status. Comparisons were performed using Wilcoxon rank-sum tests. C1-high indicates C1 ligand signature score high status, and OC-high indicates osteoclast function signature score high status.

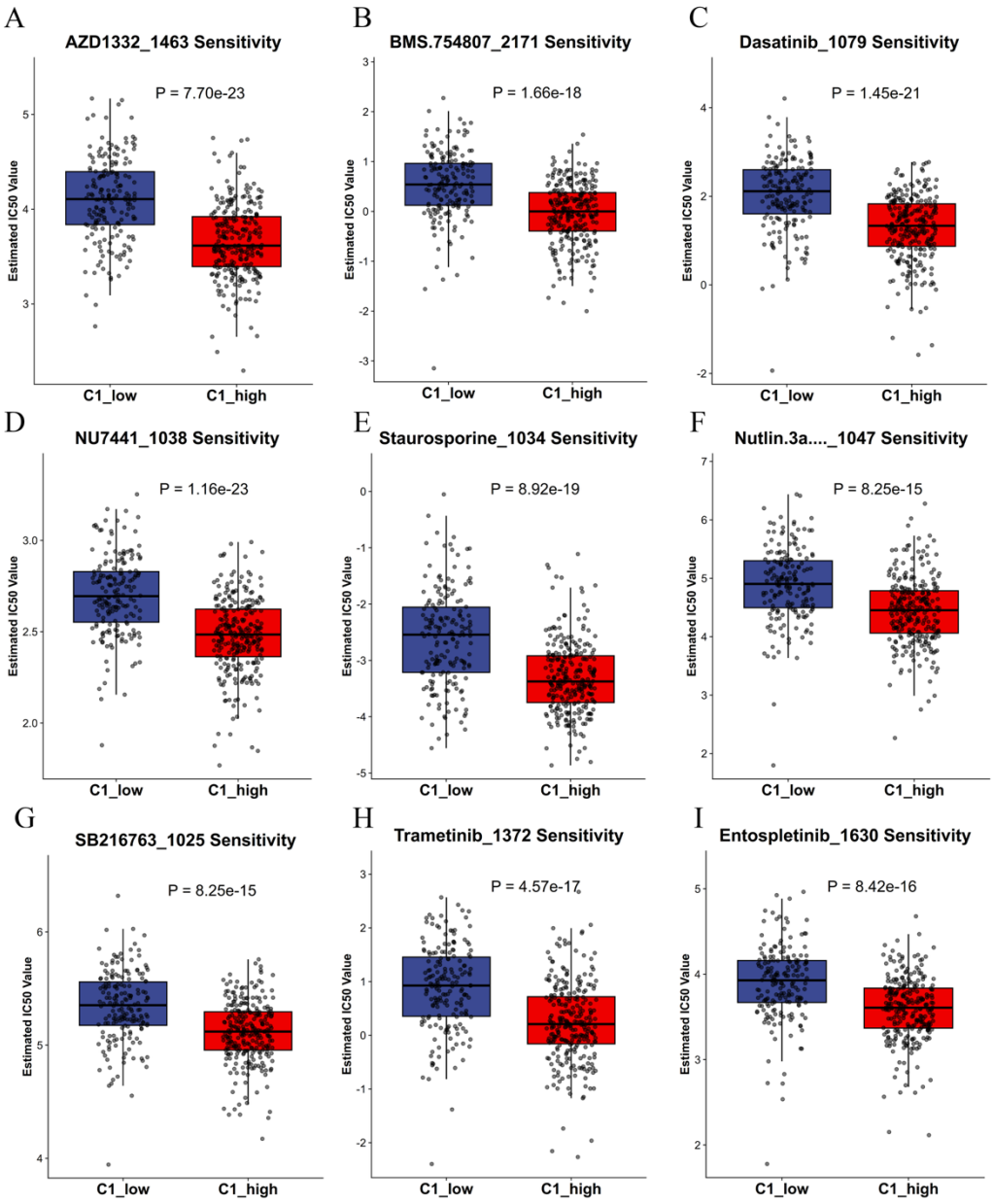

Supplementary Figure 8. Predicted drug sensitivity in C1-high and C1-low patients. A-I) Predicted IC50 values for AZD1332, BMS-754807, Dasatinib, NU7441, Staurosporine, Nutlin.3a, SB216763, Trametinib, and Entospletinib in C1 ligand signature score low and score high patients. Comparisons were performed using Wilcoxon rank-sum tests. Lower predicted IC50 values indicate higher predicted sensitivity.